Journal of Ultrafine Grained and Nanostructured Materials
https://jufgnsm.ut.ac.ir
Vol. 58, No.2, June 2025, pp. 264-276
Print ISSN: 2423-6845 Online ISSN: 2423-6837
DOI: 10.22059/jufgnsm.2025.02.11

Cytocompatibility of a 3- Dimensional Graphene Oxide/ Laminin Composite Scaffold Intended for Nerve Tissue Engineering

Khadijeh Zeinali [a], Mohammad Taghi Khorasani [b], Maryam Ataie[c]*

[a] Food and Drug Research Center, Food and Drug Administration, Ministry of Health and Medical Education, Tehran, Iran.
[b] Department of Biomaterials, Iran Polymer and Petrochemical Institute, Tehran, Iran.
[c] Faculty of Life Science Engineering, College of Interdisciplinary Science and technology, University of Tehran, Tehran, Iran.

Recieved: 29 June 2025; Accepted: 8 September 2025

[*]Corresponding author, E-mail: mariamataie1992@gmail.com

ABSTRACT

In this study, we fabricated porous and low-molecular-weight graphene oxide (GO) aerogel scaffolds via a single-step chemical reduction of GO with ethylene diamine (EDA) at 95°C for 6 hours, followed by freeze-drying. The concentrations of GO (3–8 mg/ml) and EDA (20–50 µl) were optimized using Design of Experiments (DOE) to control scaffold density and porosity. The scaffold featuring 5 mg/ml GO and 30 µl EDA exhibited optimal porous architecture with interconnected pores visible in SEM analysis and a low density of approximately 13 mg/cm^3. Laminin coating was applied to enhance biological functionality.

Biocompatibility was confirmed using MTT assays with L929 fibroblast cells, showing 124% cell viability after 72 hours, indicating no cytotoxicity and even promotion of cell proliferation. P19 mouse embryonal carcinoma cells cultured on these scaffolds successfully differentiated into neural cells, as evidenced by the expression of microtubule-associated protein-2 (MAP-2) confirmed via immunofluorescence staining. Quantitatively, neural differentiation efficiency on the scaffold reached approximately 80%, significantly higher compared to controls.

These results demonstrate that the developed GO aerogel scaffold possesses suitable mechanical properties, porosity, and bioactivity to support neural cell adhesion, proliferation, and differentiation. The scaffold's tunable density and porosity via GO and EDA concentrations provide a controllable microenvironment for neural tissue engineering applications. Future work will explore in vivo regenerative potential and electrical conductivity integration to further enhance nerve tissue repair.

Keywords: *Graphene oxide aerogel, Neural tissue engineering, Scaffold fabrication, Cell differentiation, Biocompatibility.*

1. Introduction

Damage to peripheral or central neural tissue significantly reduces patients' quality of life. Central nervous system (CNS) injuries often results in permanent loss of neurological functions, primarily because the regeneration of neural cells, especially within the spinal cord, is hindered by the formation of dense scar tissue at the injury site. This process is further complicated by physiological responses such as alterations in blood pressure, excessive release of neurotransmitters, and the death of neural cells [1]. The scar tissue hinders the growth of axons through the gaps, disrupting the structural integrity needed for proper neural signal transmission. The normal path for regeneration is the directional growth of the axons through the injury location so that physical support serves as a bridge for reconnecting severed peripheral nerves or spinal cord tissue [2]. The main limit of spinal cord regeneration is the lack of an extracellular

matrix for neural conduction to improve the function of the disconnected neural tissue. In fact, in a living creature, the cells are in a three-dimensional microenvironment surrounded by other cells and the extracellular matrix (ECM). The ECM comprises nanoscale collagen, elastin, and laminin molecules, which are organized by exclusive bioactive motifs. The extracellular matrix (ECM) plays a critical role in regulating cellular behaviors by transmitting biochemical signals and providing topographical cues. It maintains cellular homeostasis and balances cell functions. Cells residing in a three-dimensional ECM environment exhibit distinct morphological and phenotypic characteristics compared to those cultured in two-dimensional systems. Therefore, an ECM-like 3D structure offers a guiding framework that supports key cell functions such as adhesion, migration, proliferation, and differentiation. Additionally, in vitro three-dimensional models better replicate the native tissue environment, offering deeper insights into cellular processes as they occur in living organism [3, 4]. Biomaterials used to fabricate tissue engineering scaffolds contain synthetic and natural polymers, including polysaccharides, poly (α-hydroxy esters), hydrogels, and thermoplastic elastomers. In addition, the bioactive metals used for this purpose are iron alloys, silver, gold, titanium, and zinc and the nanomaterials include nano-clay, carbon nanotubes (CNTs), and graphene [5, 6].

Neural scaffolds, commonly used in neural tissue engineering for regeneration, serve multiple essential functions. They guide axonal sprouting from the nerve's origin to its target, provide adequate mechanical support for regenerating neural fibers, and act as conduits enabling the diffusion of neurotrophic and neurotropic factors released from injured nerve endings. Furthermore, these scaffolds minimize infiltration of fibrous tissue that can obstruct axonal repair and establish a micron-scale environment conducive to nerve reconstruction by regulating the accumulation and release of biochemical signals. This comprehensive functionality supports effective nerve regeneration and repair, mimicking the native extracellular matrix and microenvironment of neural tissues [10-12]. Therefore, the scaffolds must be expanded to create three-dimensional, supportive, synthetic microenvironments to control and guide cell behaviors and elicit cell-exclusive reactions. The rapid expansion of scaffold fabrication methods and the multiple amazing chemical properties of graphene and its derivatives have created many opportunities in different fields of medicine [13-16]. Graphene is a monolayer of carbon atoms in which the atoms are connected in the SP^2 layer and create a hexagonal structure (honeycomb) in a two-dimensional plate [17]. Extra-mobile carriers in single-layer graphene enable them to perfectly conduct electricity with zero band gap, which is a unique feature for non-metal materials [18]. Research shows that electronic stimulation can be useful for neural regrowth [19, 20]. The structure of graphene allows it to absorb proteins and low-molecular-weight molecules on its surface through van der Waals (due to $\pi-\pi$ interactions) and ionic bonds, increasing its application in tissue engineering. Each cell secretes substances to grow and connect to other cells, which can be absorbed to the surface of graphene and affect cell proliferation and differentiation. The use of graphene in tissue engineering has produced substantial results because of its stable chemical structure. Neural cells behave desirably next to conductive graphene due to their electroactivity and electric function. Graphene also promotes nerve sprouting and the growth of nerve processes from the cell body of immature neural cells. Graphene consists of carbon atoms arranged in a two-dimensional hexagonal lattice [21]. This is a basal block frame for other graphite materials such as several-layer graphene, GO, and reduction of graphene oxide (rGo). Several-layer graphene is a pile like the 2-to-10-layer cortex of graphene. Once the graphene undergoes oxidation, it changes chemically and is called GO. GO is a simple way to create graphene planes that include functions like hydroxyl, epoxy, carbonyl, and carboxylic. These oxygen-containing groups not only increase the dispersion of GO in different solvents but also provide the formation of other functions [16, 22-24].

Graphene is a relatively new material, and research into its use in tissue engineering is still in its early stages. Despite the limited research in this field, most of the performed activities have been satisfying. Graphene nano-substances can have a crucial role in the growth, adhesion, and cell differentiation as a cell growth medium. The main drive for this phenomenon is the ability of these nano-substances to absorb protein and low-molecular-weight substances on their surface. This kind of action is based on ionic bonds or the action between the electron clouds of graphene and proteins. After the absorption of protein on graphene nano-substances and its transfiguration, which depends on the its hydrophilicity or hydrophobicity, these nano-substances will affect the cell behavior. Moreover, graphene nano-substances can be applied to strengthen other scaffold substances, and many studies are undergoing [19, 25]. As mentioned earlier, graphene can lead to the differentiation of stem cells into neural cells alone. Meng et al. studied the effect of constant electrical stimulation to modify cell behavior and improve tissue repair by placing

a graphene film on a polyurethane substrate using a spray coating method and examining the effect of intensity, duration, frequency, pulse, and the time distance of electric stimulations on cell differentiation. They reported that this approach could be applied to improve differentiation in other composites [26].

Although pristine graphene can promote synaptogenesis and support the stable growth of nerve cells, its smooth surface, chemical inertness, and lack of biological recognition sites limit its ability to effectively interact with and guide peripheral nerves within living organisms [7, 27, 28]. Nanostructures, including fibers, grooves, and threads, have been found to increase cellular attachment and new tissue proliferation, while proliferation induced by growth factors increases the growth and alignment of neural cells [29, 30]. Moreover, π-πstrong bonds are the direct specifiers of aromatic accumulations on the graphene surface. This hypothesis holds that bacterial interaction with cell membranes is a serious damaging factor. Currently, a significant portion of high-quality pure graphene is produced using the chemical vapor deposition (CVD) method. However, this technique demands substantial energy input due to the high temperatures required, rendering it both costly and environmentally challenging [31]. Therefore, graphene derivatives have been modified to produce different nanocomposites, such as GO, to improve surface roughness and increase neural growth [29, 32-34]. For example, considering the high mobility of charge carriers in graphene, different parts of its structure can be proportionate for connecting to a neural grid by charging different surfaces, which shows the neural levels for nerve length increase and general growth [35]. Moreover, graphene nanocomposites are suitable to be loaded into growth factors or drugs and provide ways for connecting to various biomolecules, such as proteins, carbohydrates, and nucleic acids [20, 36, 37]. These various forms of graphene nanocomposites and their high electrical capability allows graphene to collect and register neural system's complex signaling processes by functioning as an electrode.

Different methods have been employed to fabricate geraphene based scaffolds such as freeze-drying, ice segregation-induced self-assembly (ISISA), solvent casting, gas foaming, melt moulding, emulsification, electrospinning and bioprinting. Scaffolds fabricated via freeze-drying benefit from thermal stability, apt hydrophilicity, biocompatibility, good porosity, and improved morphology to stimulate cell growth. Good porosity and interconnectivity enable easy microvasucularizations while some inflammatory responses have been reported [38].

This study presents the development of a novel porous, low-molecular-weight GO aerogel scaffold fabricated via a single-step chemical reduction using EDA followed by freeze-drying, designed to mimic the mechanical properties of native nerve tissue for neural regeneration. The scaffold was optimized for porosity and density through experimental design methods and coated with laminin to enhance bioactivity. Characterization by SEM and FTIR confirmed a three-dimensional interconnected porous structure with appropriate chemical functionalities. Biological assessments demonstrated excellent biocompatibility, fibroblast adhesion, and the ability to support P19 mouse stem cell differentiation into neural cells, confirmed by immunofluorescence for neural marker MAP-2. These findings highlight the scaffold's promising mechanical and biological properties, making it a suitable candidate for nerve tissue engineering and regeneration applications

2. Materials and methods

2.1. Materials

The materials included graphite, H_2SO_4, EDA, 96% ethanol, glutaraldehyde with (Merck Co.), potassium permanganate $KMnO_4$, hydrochloric acid (HCL), hydrogen peroxide (H_2O_2), retinoic acid (RA), MAP-2 antibody (Sigma-Aldrich, U.S.).

2.2. Experimental design

Design of Experiments (DOE) methodologies are widely employed to identify and optimize critical variables and assess their effects on experimental outcomes. Traditional approaches, particularly Full Factorial Design (FFD), can be complex and often inefficient when numerous factors are involved, requiring extensive experimental runs. To address these limitations, modern DOE designs, such as those implemented in specialized software like Design Expert (Version 11), have gained prominence for their efficiency and robustness. In this study, GO and EDA concentrations were selected as cross-linking factors, with ranges of 3 to 8 mg/ml and 20 to 50 µl, respectively. Six levels for GO and four for EDA were chosen, resulting in 16 experimental runs as suggested by the software (Table 1).

The optimal predictive model was selected based on the coefficient of determination (R^2). Additionally, analysis of variance (ANOVA) was conducted using mean square values, residual errors, and regression analysis to evaluate the statistical significance and adequacy of the model. Relevant details of the experimental design and statistical analysis are summarized in Table 2.

Design of Experiments (DOE) methods are commonly used to identify and optimize critical variables, as well as to evaluate their effects on

Table. 1- Used and the levels of variables in each experiment in the experimental design

Sample number	Graphene oxide (mg/ml)	Ethylene diamine (µl)	Sample number	Graphene oxide (mg/ml)	Ethylene diamine (µl)
1	3	30	9	8	20
2	8	40	10	5	50
3	7	30	11	6	40
4	3	20	12	8	20
5	3	50	13	4	40
6	3	20	14	7	50
7	7	50	15	5	30
8	3	50	16	8	40

Table. 2- The data of the experimental designing method

File Version	11.0.3.0		
Study Type	Response Surface	Subtype	Randomized
Design Type	D-optimal	Runs	16
Design Model	Quadratic	Blocks	No Blocks
Build Time (ms)	1.0000		

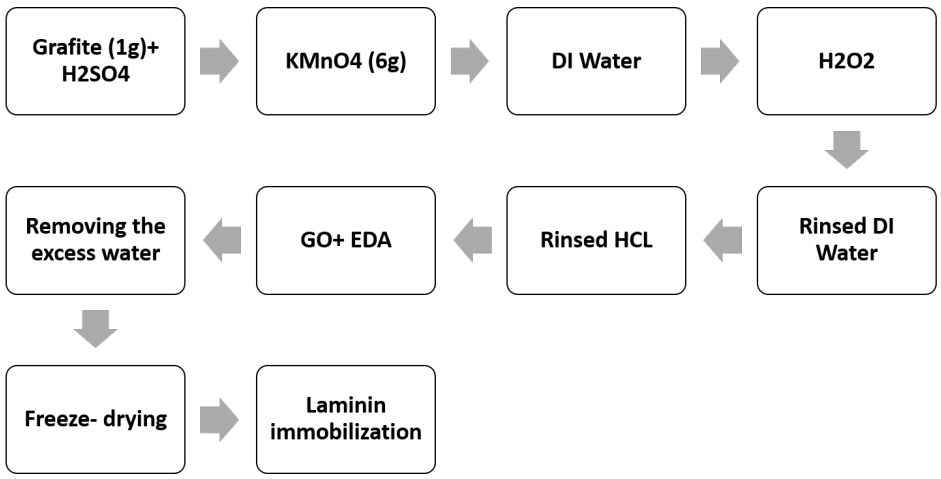

Fig. 1- The GO preparation steps according to the modified Hummer's method.

outcomes. Traditional approaches, especially Full Factorial Design (FFD), tend to be complex and often inefficient when many variables are involved, necessitating a high number of experiments. To overcome these challenges, various alternative experimental designs have been developed, among which the methodology implemented in Design Expert software has gained considerable attention. In this study, the experimental design was created using Design Expert (Version 11), with graphene oxide (GO) and ethylene diamine (EDA) concentrations set as cross-linking factors ranging from 3 to 8 mg/ml and 20 to 50 µl, respectively. Six and four levels were selected for GO and EDA, leading to 16 experimental runs as suggested by the software (Table 1).

The most suitable model was selected based on the coefficient of determination (R^2). Furthermore, an analysis of variance (ANOVA) was performed using mean square, residual error, and regression values to assess the significance and adequacy of the model. Table 2 summarizes the details of the experimental design and analysis.

2.3. Scaffold fabrication

2.3.1. Synthesis of GO

Fig.1. shows the process of scaffold fabrication. The color of each box represents the product color during the reaction steps. 1 g of graphite was added to 80 ml of concentrated H_2SO_4 then, 6 g of potassium permanganate (a_4) was gently added to the resulting solution. The solution was kept stirring at 20°C after the addition of $KMnO_4$ overnight. In the following, the color of the solution changed from greenish brown to brownish yellow by adding H_2O_2 to the system. The solution was centrifuged at 4000 rpm for ten min to separate the graphite oxide from the reaction mixture. The resulting substance was rinsed with distilled water and HCL five times to separate the acid and salts of the reaction mixture from the graphite oxide. To prepare GO, the obtained graphite oxide was poured into the water first and mixed using ultrasonic waves for 1 h. Once the sonication was finished, a light brown homogeneous mixture was obtained [39-41].

2.3.2. Preparing GO aerogel

5 ml of suspended GO with different concentrations and the desired volume of EDA were added to the glass tube and placed on a shaker at 200 rpm for 1 min followed by placing in the ultrasonic homogenizer for 2 min under the power of 80 watts and with pulses of 0.5 seconds to 0.5 seconds. The container was sealed using teflon tape then placed in the oven (95°C for 6 h). The suspension became dark blue and remained homogeneous, indicating chemical reduction. A black cylinder floated until the top of the suspended solution was formed. After the reaction completion, the excess water was removed to prevent entering the hydrogel grid. In the first step of reduction, some of the graphene sheets appear from the same reduced amount, in which the hydrophobicity of graphene sheets leads to aggregation, which agrees with the reported results [42-45]. As the reaction continues, the hydrophobicity and π-π conjugated structures of the reduced GO sheets increased. By the end, a compressed three-dimensional structure can be created due to the spatial hindrance effect of graphene sheets in micrometer diameters. Also, the hydrogel was rinsed with double distilled water every 4 h for at least 48 h to ensure that the unreacted EDA has been removed. It was finally freeze-dried for 24 h [46, 47].

2.3.3. immobilization of laminin on the surface of the scaffold

After preparing the scaffolds, they were rinsed with physiological serum several times, and twice with distilled water. 300 µl of L2020 laminin was dissolved in 3 ml of double distilled water. The scaffolds were then soaked in laminin solution followed by drying.

2.4. scaffold characterization

In order to compare the effect of cross-linker and the polymer concentration on the density of the samples, the pycnometer measuring method was used. To this aim, Polyethylene glycol (PEG) with a molecular weight of 400 was used. It is worth mentioning that the solvent density was measured at the test temperature first, as density is temperature dependent. Also, the applied pycnometer had a volume of 10 ml.

The AIS210 scanning electron microscope (SEM; SERON TECHNOLOGY, South Korea) was used to examine the cross-sectional morphology of the scaffolds after coating by gold sputter coater device (SC7620, QUORUM TECHNOLOGIES-EMITECH, U.K.).

To identify the bonds and chemical structure of graphene sheets Fourier transform infrared spectroscopy (FTIR; Thermo Nicolet, NEXUS 870, 400-5000 cm^{-1}) was used.

2.5. biological evaluations

P19 mouse cells were used to assess the suitability of the fabricated hybrid scaffolds for supporting neural cell growth. The P19 cell line used in this study was obtained from the Genetics Institute of Iran. Initially, frozen aliquots of P19 cells were rapidly thawed at 37°C and cultured under standard conditions in α-MEM (GIBCO, Germany) supplemented with 10% fetal bovine serum (FBS), 100 IU/ml penicillin, and 100 µl/ml streptomycin. The cells were incubated at 37°C

(5% CO_2), and the culture medium was refreshed every 48 hours. The cells were then transferred to 100 mm bacteriological culture dishes. At this point (day 0), the culture medium consisted of α-MEM supplemented with 10% FBS and 0.3 μM retinoic acid (Sigma). The culture continued for four days, with the medium refreshed every 48 hours. During this time, multiple cell aggregates were formed. These aggregates were mechanically dissociated and then seeded into specialized culture vessels containing the hybrid scaffolds in a retinoic acid-free medium. Cultivation proceeded for an additional ten days, totaling fourteen days in culture.

Cell growth and differentiation were monitored regularly using optical microscopy, while parallel dishes without scaffolds served as negative controls to observe baseline cell proliferation. After 14 days, the culture medium was gently aspirated to stabilize the cells adhered to the scaffolds. The scaffolds were then washed for five minutes to remove non-viable cells, rinsed with phosphate-buffered saline (PBS), and dehydrated through sequential immersion in graded ethanol-water solutions (90%, 80%, 70%, 60%, 50%, and 100%) for five minutes each. Following another PBS wash, the scaffolds were air-dried at room temperature for 24 hours.

Finally, after the differentiation of P19 cells on the hybrid scaffolds, the samples were analyzed using scanning electron microscopy (SEM) and optical light microscopy to assess cell morphology and interactions with the scaffold.

The cell attachment on the scaffolds was observed using SEM to examine the interaction of cells and scaffold after 24 hours. to this aim, 6 ml of 25% glutaraldehyde was added to 44 ml of distilled water. Then, 8.4 ml of the mentioned solution was added to each scaffold. The scaffold-containing plate was placed in an incubator for 15 min followed by dehydration in ethanol gradient and drying to be investigated by SEM.

The biocompatibility of the samples was evaluated using methylthiazolyl diphenyl tetrazolium bromide (MTT, Sigma) based on our previous study [47]. Briefly, the L929 fibroblast cells were cultured in a DMEDM2 medium containing 10% fetal bovine serum (FBS), and 1% streptomycin/penicillin. All cellular examinations were performed on each cell of this test in a moist, 5% CO_2-containing medium at 37°C after sterilizing the samples with an ultraviolet ray for half an hour. DMEM medium (high glucose level) enriched by 10% FBS and 1% penicillin/streptomycin was used for NIH-3T3 fibroblast cells.

The suitability of the hybrid scaffolds as a medium for the growth of neural cells was validated using P19 mouse cells. The P19 cell line was supplied by the Genetics Institute of Iran. The frozen P19 cell package was rapidly thawed at 37°C. The cells were maintained in the standard environment containing α-MEM (GIBCO, Germany) with 10% FBS, and were supplemented with 100 IU/ml Penicillin and 100μl/ml Streptomycin. The cells were then incubated at 37°C (5% CO_2) during which the culture medium was refreshed every 48 h until the number of cells reached 10^4×5 cell/ml. The cells were transferred to 100 mm bacteriological containers. The culture medium consisted of 10% FBS, α MEM (GIBCO), and 0.3μM RA (Sigma) in 100mm bacteriological Petri dishes. The cell culture was carried on four days during which the medium was refreshed every 48 h.

Multiple cell aggregates were mechanically separated. Then, special cell cultures were provided, which consisted of hybrid scaffolds in a non-retinoic acid environment, in which the mechanically separated aggregates were placed. The cultivation was carried on for another ten days (a total of fourteen days). An optical microscope was used to monitor the growth and differentiation of cells. Accordingly, the cultivation dishes were treated as the positive control to reflect cell growth.

At the end of the 14th day, the culture medium was gently discharged to stabilize the grown cells on the hybrid scaffold. The dead cells were then washed off the hybrid scaffolds for 5 min. The samples were washed with PBS for 5 min and dehydrated by immersion in a series of ethanol-water solutions with 90, 80, 70, 60, 50, and 100% v/s for 5 minutes in each alcohol. They were then washed for another 5 min. Ultimately; the hybrid scaffolds were exposed to ambient temperature for 24 h to dry. After the culturing and differentiating stages of the P19 cells into scaffolds, an SEM analysis was performed [47].

To study the differentiation of P_{19} cells to neural cells on the prepared scaffolds monoclonal antibody, which is a specialized antibody for recognizing MAP-2, was used. To confirm the presence of cells in newly created layers, a fluorescent microscope was used. The stabilized cell-containing scaffolds were evaluated by DAPI staining.

3. Results and Discussion

In addition to reporting the experimental outcomes, it is essential to clarify the mechanisms underlying the observed changes in scaffold properties. The variation in GO and EDA concentrations directly influences scaffold density and porosity. Increasing GO concentration enhances nucleation density, leading to denser microstructures, while EDA contributes to crosslinking through amine–epoxy and amine–carboxyl interactions, which regulate pore size and distribution. Moreover, π–π stacking interactions among reduced GO sheets promote

aggregation and improve structural stability, thereby enhancing compressive strength and long-term integrity of the scaffold [48, 49]. Laminin coating further strengthens the biological performance by presenting cell-binding motifs that interact with integrins, facilitating fibroblast adhesion and promoting neural differentiation [16, 20]. Additionally, the three-dimensional porous microarchitecture provides interconnected channels that allow nutrient diffusion and cell infiltration, both of which are critical for supporting sustained proliferation and neural differentiation [13, 50].

The density is among the important properties affecting the function of the scaffold and all other features including the mechanical strength. Primary percent composition modeling was performed on the amount of density. The software suggested the Quartic model based on this data. Fig.2 indicates the three-dimensional analysis of the relationship between the amounts of GO and EDA with density. The initial nucleolus of aerogel is made of graphene plates, and it is expected that by increasing the concentration of graphene in the system, its density will increase as well. The amount of applied EDA and the ratio of graphene to EDA is another factor, which has a direct effect on the density [49, 51].

A summary of the statistical details of the model is mentioned in Table 3. Fig.2 indicates the analysis of this model. The maximum density is approximately 8 mg/ml for GO and formed in sample 12 (i.e. 8 mg/ml GO, 20 µl EDA), the highest rate of graphene.

Fig.3 shows the GO and GO/Laminin aerogel spectrum. Fig.3 shows the absorption peaks originated from oxide groups localized on GO. The peak appeared in 3443 cm^{-1} is related to flexural (bending) vibrations of O-H groups and the peak appeared at 1739 cm^{-1} corresponds to tensile vibrations of C=O groups in carbonyl and carboxyl groups; the peak at 1568 cm^{-1} reveals tensile vibrations of aromatic carbon C=C; at 1467 cm^{-1} tensile vibrations of the carboxyl group of C-O existing in –COOH are seen; the peak at 1089 cm^{-1} represents the tensile vibrations of epoxy groups (1 and -2 ether), and finally the peak appeared at 544 cm^{-1} is attributed to the change in the form of the C-H group attached to C = C. The presence of these functional groups causes the GO polarization, which justifies the ease of homogeneous distribution in the water [48, 52]. According to the structure of Laminin, the carbonyl amide peak at 1637 cm^{-1} in the Laminin-containing scaffold.

Fig.4 shows the SEM images illustrate the honeycomb porous structure of GO aerogel plates of sample 15; Pore diameters are shown on the image. As observed, the distances between the layers can be tens of micrometers [21], which shows the creation of a three-dimensional, interconnected, porous grid with high compressive strength. The images of the GO aerogel cross-section show the wide range of structure porosity.

The SEM images clearly display the overall structure, interaction, and adhesion of cells to the samples. The interconnection between cells is well demonstrated in the scaffold images. It is more

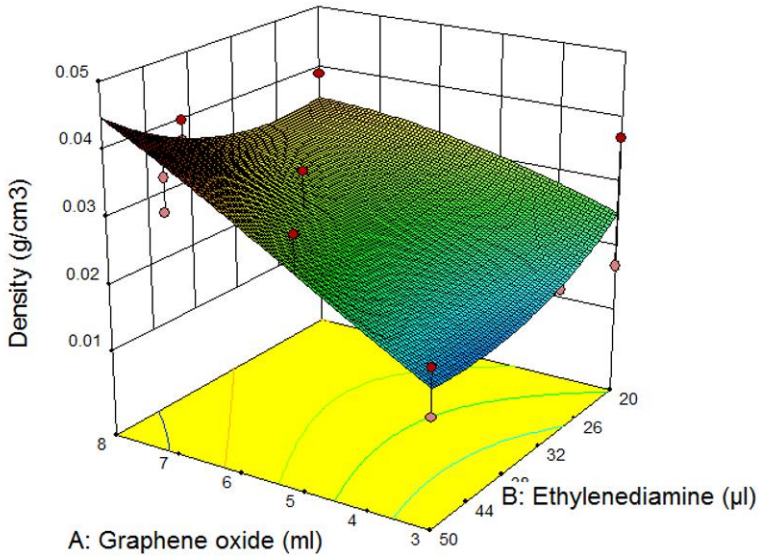

Fig. 2- The three-dimensional analysis of the relationship between the amounts of GO and EDA with density.

Table. 3- A summary of the statistics of the model

ANOVA for Response Surface Quadratic model						
Analysis of variance table [Partial sum of squares - Type III]						
	Sum of		**Mean**	**F**	**p-value**	
Source	**Squares**	**df**	**Square**	**Value**	**Prob > F**	
Model	**8.497E-003**	**5**	**1.699E-003**	**4.40**	**0.0222**	**significant**
A-Graphene oxide	**7.526E-003**	**1**	**7.526E-003**	**19.51**	**0.0013**	
B-Ethylenediamine	**1.225E-005**	**1**	**1.225E-005**	**0.032**	**0.8622**	
AB	**1.199E-003**	**1**	**1.199E-003**	**3.11**	**0.1084**	
A2	**7.233E-005**	**1**	**7.233E-005**	**0.19**	**0.6742**	
B2	**3.630E-004**	**1**	**3.630E-004**	**0.94**	**0.3550**	
Residual	**3.858E-003**	**10**	**3.858E-004**			
Lack of Fit	**1.151E-003**	**5**	**2.301E-004**	**0.42**	**0.8154**	**not significant**
Pure Error	**2.708E-003**	**5**	**5.415E-004**			
Cor Total	**0.012**	**15**				

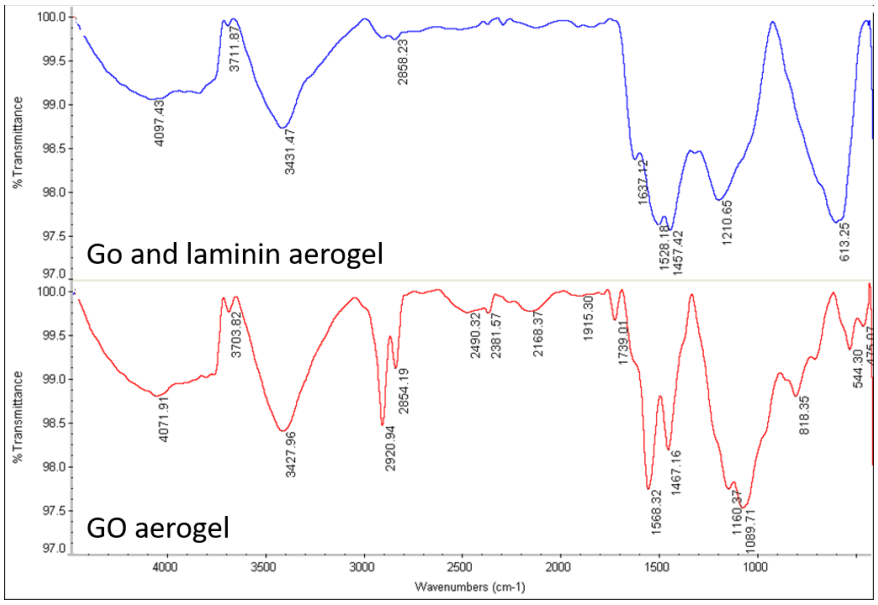

Fig. 3- FTIR spectrum of GO and GO/ Laminin aerogel.

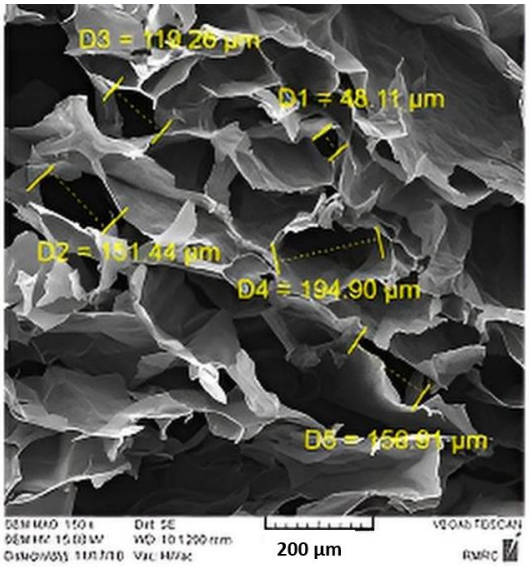

Fig. 4- The SEM image of GO aerogel (sample 15- pore diameters are shown on the image).

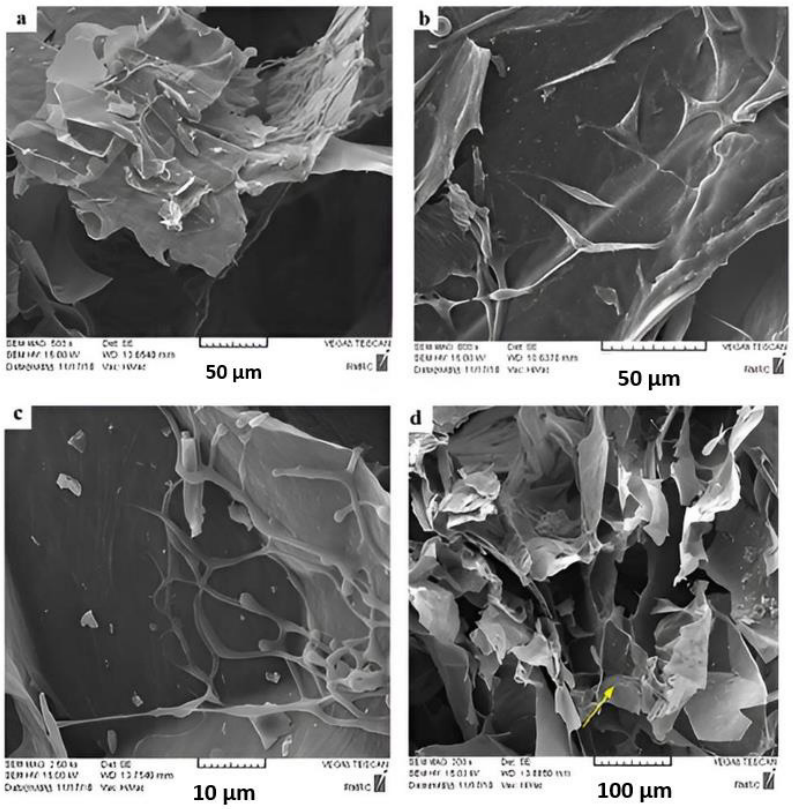

Fig. 5- (a) SEM image of GO aerogel scaffold surface prepared through fibroblast cell culture after 72 hours (b), (c), and (d) electron microscope images of the cross-section of GO aerogel scaffold prepared through fibroblast cell culture after 72 hours in different magnifications.

difficult to take appropriate images in the scaffolds due to their porous structure and the penetration of cells therein.

Fig.5 shows that the cells are completely overspread on the compositional scaffold surface, and the cells' filopodia are clearly visible. According to Fig.5 (b, c, and d), the fibroblast cells are highly able to infiltrate and migrate to inner parts, which proves the biological uniformity.

Fig.6 specifies the MTT test results of scaffolds and the control group following 72 h of cell culturing. All the samples fabricated in this study were biocompatible after 72 h which implies lack of toxicity in L-929 cells. Cell viability and the L-929 cell contact were 124%.

Fig.7 shows the SEM images of differentiated mouse P19 cell on the scaffold after 14 days at different scales. Blue dots represent the live cells. According to Fig.7, a completely new layer is visible on the scaffolds. As mentioned before, the cell cultivation operation was performed statically in this research, which is not the best condition for tissue formation, since a layer of cells has formed on the scaffold and does not allow the other cells or even the nutrients to enter the scaffold, and the captivated cells might also get destroyed.

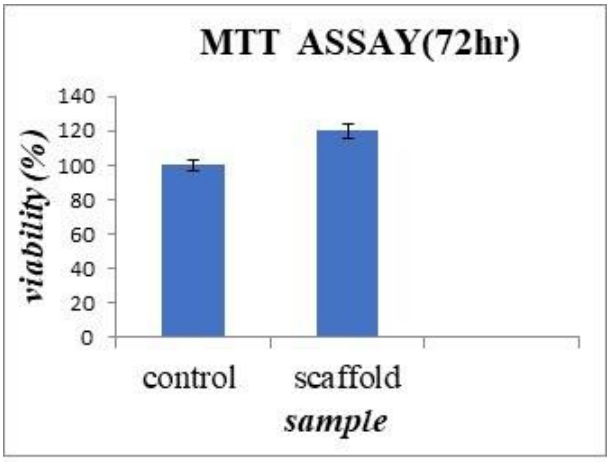

Fig. 6- Cell viability percentage after 72h cell culture on the surface of the scaffold in comparison with the control group.

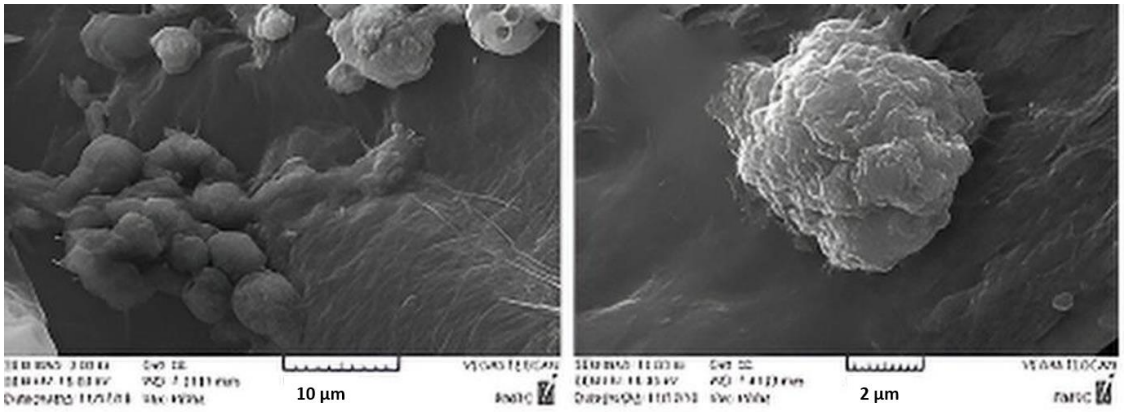

Fig. 7- The SEM images of differentiated mouse P19 cell on the scaffold after 14 days at different scales. Blue dots represent the live cells.

An objective was to prove the P19 cell's ability to differentiate into neural cells on the prepared scaffolds. To this aim, a specified test was required to prove that the obtained cells through this process are neural. Accordingly, a monoclonal antibody specialized to recognize MAP-2 was used. MAP-2 is a special protein in neural cells. Fig.8 represents the fluorescence imaging of the cells marked with MAP-2 antibody on the scaffold after 14 days of culturing; The blue dots represent cells. (a) nuclei stained by DAPI, (b) primary antibody to MAP-2, (c) merge, magnification: 400×, Positive reaction: 80.2%.

Another specified test was performed to examine the differentiation of P19 mouse cells into neural cells in addition to confirming the formation of neural tissue on the scaffolds. Since different cell classes produce their special proteins, in other words, peptides, an accurate evaluation of the cell-made environment around vital cells can provide precise information about the type of cells. Therefore, the specified antibody was used to identify the MAP-2 protein. MAP-2 is a neural-cell-specified protein. It must be noticed that the images of the fluorescent microscope were taken by coloring the nucleus of desired P19 cells after 14 days of loading inside the scaffold, and the observed green color in the images is the fluorescent light reflected by the scaffold. The figures show that the MAP-2 antibody-marked cells were visible by the microscope. The neon green dots in Fig.8 is the regions that have shown a positive reaction to the special antibody due to the existence of MAP-2 protein and have been observed and registered by the microscope. The presence of this protein, a special neural cell protein, proves that P19 cells are well differentiated from neural cells after the steps of cultivation and cellular modification.

The combination of in vitro cell cultivation experiments and immunofluorescence tests showed that the prepared scaffolds are appropriate for P19 cell adhesions, formation of cell aggregations, and establishing connections between cells and their differentiation. Also, the obtained piped morphology through the phase separation method is a suitable structure for neural cell infiltration and growth. Besides the positive reaction of cells to the immunofluorescence test, the intensity of this reaction is also important. The series of cell cultivation reactions, DAPI, and immunofluorescence tests showed that the prepared scaffolds are suitable for the adhesion of P19 mouse cells, establishing connections between cells, formation of cell aggregations, and their differentiation to neural cells.

Previous researches have been performed on laminin modified geraphene oxide for neural tissue engineering. Kang et al. fabricated the nanofibre composite matrices of poly(L-lactide-co-ε-caprolactone) (PLCL) and laminin (Lam) functionalized with graphene oxide (GO) (PLCL/Lam/GO). They observed the potential of the scaffolds to enhance cell adhesion, proliferation the differentiation of hippocampal neuronal cells [53]. Qian Y et al. intend to fabricate a GO based PCL scaffold modified by laminin to investigate the potential compatibility of the scaffold for Schwann cells in the peripheral nerve tissue engineering. The biocompatible nerve scaffold was seen to be beneficial to nerve regeneration [54].

In addition to reporting the experimental results, it is important to clarify the mechanisms that underlie the observed changes. The variation in GO and EDA concentrations directly influences scaffold density and porosity. Higher GO concentrations increase nucleation density, leading to denser scaffolds, while EDA acts as a crosslinker through amine-epoxy and amine-carboxyl interactions, modifying the pore architecture. Furthermore, π–π stacking interactions among reduced GO sheets contribute to aggregation and structural stability, thereby affecting the compressive strength. Laminin coating enhances scaffold bioactivity by providing cell-binding motifs that interact with integrins, facilitating fibroblast adhesion and promoting neural differentiation. The porous 3D architecture further provides channels for nutrient transport and space for cell infiltration, which are

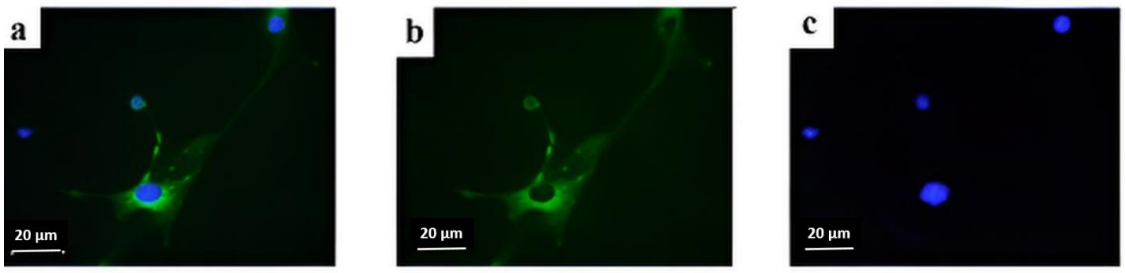

Fig. 8- Fluorescence imaging of the cells marked with MAP-2 antibody on the scaffold after 14 days of culturing, (a) nuclei stained by DAPI, (b) primary antibody to MAP-2, (c) merge, magnification: 400×, Positive reaction: 80.2%.

critical for long-term tissue regeneration. Our findings can also be placed into the context of other practical works in the field. For instance, Zhang et al. demonstrated that aligned PLLA nanofibrous scaffolds coated with GO promoted neural growth, while Song et al. reported enhanced cell adhesion using GO-based polycaprolactone composites [29, 34]. Similarly, Chiacchiaretta et al. showed that GO could modulate astrocyte-to-neuron communication, and laminin-functionalized GO scaffolds supported Schwann cell compatibility in peripheral nerve regeneration [32]. Compared to these studies, our scaffolds achieved higher neural differentiation efficiency (~80%), which we attribute to the synergistic optimization of scaffold porosity, density control through GO/EDA ratios, and laminin coating. This positions our work as a step forward in developing effective GO-based scaffolds for neural tissue engineering.

4. Conclusion

This study reports the successful fabrication of porous and low-molecular-weight GO aerogel scaffolds using a single-step chemical reduction with EDA, followed by freeze-drying and laminin coating for enhanced bioactivity. Scaffold composition was systematically optimized for density and porosity via design of experiments, resulting in a tunable microarchitecture with interconnected pores and low density (13 mg/cm^3). The scaffolds exhibited excellent biocompatibility, confirmed by high cell viability (124%) in fibroblast cultures, and effectively supported neural differentiation demonstrated by 80% efficiency in converting P19 mouse embryonal carcinoma cells into neural cells as verified by MAP-2 immunofluorescence. Collectively, these engineered scaffolds demonstrate promising mechanical and biological properties for neural tissue engineering and regeneration applications, with control over microenvironment features, strong fibroblast adhesion, and robust neural cell support.

References

1. Ba, M. and F. Bonhoeffer, Perspectives on axonal regeneration in the mammalian CNS. Trends in neurosciences, 1994. 17(11): p. 473-479.
2. Silver, J. and J.H. Miller, Regeneration beyond the glial scar. Nature reviews neuroscience, 2004. 5(2): p. 146-156.
3. Gu, X., F. Ding, and D.F. Williams, Neural tissue engineering options for peripheral nerve regeneration. Biomaterials, 2014. 35(24): p. 6143-6156.
4. López-Dolado, E., et al., Subacute tissue response to 3D graphene oxide scaffolds implanted in the injured rat spinal cord. Advanced healthcare materials, 2015. 4(12): p. 1861-1868.
5. Misra, S.K., et al., Poly (3-hydroxybutyrate) multifunctional composite scaffolds for tissue engineering applications. Biomaterials, 2010. 31(10): p. 2806-2815.
6. Peter, M., et al., Novel biodegradable chitosan–gelatin/nano-bioactive glass ceramic composite scaffolds for alveolar bone tissue engineering. Chemical engineering journal, 2010. 158(2): p. 353-361.
7. Li, N., et al., Three-dimensional graphene foam as a biocompatible and conductive scaffold for neural stem cells. Scientific reports, 2013. 3(1): p. 1-6.
8. Dastjerdi, R. and M. Montazer, A review on the application of inorganic nano-structured materials in the modification of textiles: focus on anti-microbial properties. Colloids and surfaces B: Biointerfaces, 2010. 79(1): p. 5-18.
9. Karimi, Z., L. Karimi, and H. Shokrollahi, Nano-magnetic particles used in biomedicine: Core and coating materials. Materials Science and Engineering: C, 2013. 33(5): p. 2465-2475.
10. Hudson, T.W., G.R. Evans, and C.E. Schmidt, Engineering strategies for peripheral nerve repair. Orthopedic Clinics, 2000. 31(3): p. 485-497.
11. Evans, G.R., Peripheral nerve injury: a review and approach to tissue engineered constructs. The Anatomical Record: An Official Publication of the American Association of Anatomists, 2001. 263(4): p. 396-404.
12. Johnson, E.O. and P.N. Soucacos, Nerve repair: experimental and clinical evaluation of biodegradable artificial nerve guides. Injury, 2008. 39(3): p. 30-36.
13. Shin, S.R., et al., Graphene-based materials for tissue engineering. Advanced drug delivery reviews, 2016. 105: p. 255-274.
14. Aydin, T., et al., Graphene based materials in neural tissue regeneration. Cell Biology and Translational Medicine, Volume 3, 2018: p. 129-142.
15. Yang, K., et al., The influence of surface chemistry and size of nanoscale graphene oxide on photothermal therapy of cancer using ultra-low laser power. Biomaterials, 2012. 33(7): p. 2206-2214.
16. Lee, W.C., et al., Origin of enhanced stem cell growth and differentiation on graphene and graphene oxide. ACS nano, 2011. 5(9): p. 7334-7341.
17. Allen, M.J., V.C. Tung, and R.B. Kaner, Honeycomb carbon: a review of graphene. Chemical reviews, 2010. 110(1): p. 132-145.
18. Sotoudeh, A. and M. Amirmazlaghani, Graphene-based field effect diode. Superlattices and Microstructures, 2018. 120: p. 828-836.
19. Ryu, S. and B.-S. Kim, Culture of neural cells and stem cells on graphene. Tissue Engineering and Regenerative Medicine, 2013. 10(2): p. 39-46.
20. Goenka, S., V. Sant, and S. Sant, Graphene-based nanomaterials for drug delivery and tissue engineering. Journal of Controlled Release, 2014. 173: p. 75-88.
21. Novoselov, K.S., et al., Electric field effect in atomically thin carbon films. science, 2004. 306(5696): p. 666-669.
22. Zhang, L. and T.J. Webster, Nanotechnology and nanomaterials: promises for improved tissue regeneration. Nano today, 2009. 4(1): p. 66-80.
23. Dvir, T., et al., Nanotechnological strategies for engineering complex tissues. Nano-Enabled Medical Applications, 2020: p. 351-382.
24. Farokhzad, O.C. and R. Langer, Impact of nanotechnology on drug delivery. ACS nano, 2009. 3(1): p. 16-20.
25. Nardecchia, S., et al., Three dimensional macroporous architectures and aerogels built of carbon nanotubes and/or graphene: synthesis and applications. Chemical Society Reviews, 2013. 42(2): p. 794-830.
26. Meng, S., Nerve cell differentiation using constant and programmed electrical stimulation through conductive non-functional graphene nanosheets film. Tissue Engineering and Regenerative Medicine, 2014. 11(4): p. 274-283.
27. Tang, M., et al., Enhancement of electrical signaling in neural networks on graphene films. Biomaterials, 2013. 34(27): p. 6402-6411.
28. Pampaloni, N.P., et al., Sculpting neurotransmission during synaptic development by 2D nanostructured interfaces.

Nanomedicine: Nanotechnology, Biology and Medicine, 2018. 14(7): p. 2521-2532.
29. Zhang, K., et al., Aligned PLLA nanofibrous scaffolds coated with graphene oxide for promoting neural cell growth. Acta biomaterialia, 2016. 37: p. 131-142.
30. Huang, C., et al., Nerve guidance conduits from aligned nanofibers: improvement of nerve regeneration through longitudinal nanogrooves on a fiber surface. ACS applied materials & interfaces, 2015. 7(13): p. 7189-7196.
31. Novoselov, K.S., et al., A roadmap for graphene. nature, 2012. 490(7419): p. 192-200.
32. Chiacchiaretta, M., et al., Graphene oxide upregulates the homeostatic functions of primary astrocytes and modulates astrocyte-to-neuron communication. Nano letters, 2018. 18(9): p. 5827-5838.
33. Akhavan, O., et al., Accelerated differentiation of neural stem cells into neurons on ginseng-reduced graphene oxide sheets. Carbon, 2014. 66: p. 395-406.
34. Song, J., et al., The preparation and characterization of polycaprolactone/graphene oxide biocomposite nanofiber scaffolds and their application for directing cell behaviors. Carbon, 2015. 95: p. 1039-1050.
35. Tu, Q., et al., Effects of surface charges of graphene oxide on neuronal outgrowth and branching. Analyst, 2014. 139(1): p. 105-115.
36. Kuila, T., et al., Chemical functionalization of graphene and its applications. Progress in Materials Science, 2012. 57(7): p. 1061-1105.
37. Weaver, C.L. and X.T. Cui, Directed neural stem cell differentiation with a functionalized graphene oxide nanocomposite. Advanced healthcare materials, 2015. 4(9): p. 1408-1416.
38. Geetha Bai, R., et al., Graphene-based 3D scaffolds in tissue engineering: fabrication, applications, and future scope in liver tissue engineering. International journal of nanomedicine, 2019: p. 5753-5783.
39. Chen, J., et al., Synthesis of graphene oxide sheets with controlled sizes from sieved graphite flakes. Carbon, 2016. 110: p. 34-40.
40. Nourmohammadi, A., et al., Graphene oxide sheets involved in vertically aligned zinc oxide nanowires for visible light photoinactivation of bacteria. Journal of alloys and compounds, 2014. 612: p. 380-385.
41. Rahmani, Z., et al., Nanoporous graphene and graphene oxide-coated polyurethane sponge as a highly efficient, superhydrophobic, and reusable oil spill absorbent. Journal of environmental chemical engineering, 2017. 5(5): p. 5025-5032.
42. Hu, H., et al., The role of microwave absorption on formation of graphene from graphite oxide. Carbon, 2012. 50(9): p. 3267-3273.
43. Hu, H., et al., Ultralight and highly compressible graphene aerogels. Advanced materials, 2013. 25(15): p. 2219-2223.
44. Chen, W. and L. Yan, In situ self-assembly of mild chemical reduction graphene for three-dimensional architectures. Nanoscale, 2011. 3(8): p. 3132-3137.
45. Xu, Y., et al., Self-assembled graphene hydrogel via a one-step hydrothermal process. ACS Nano, 2010. 4(7): p. 4324-30.
46. Schaedler, T.A., et al., Ultralight metallic microlattices. Science, 2011. 334(6058): p. 962-965.
47. Li, J., et al., Ultra-light, compressible and fire-resistant graphene aerogel as a highly efficient and recyclable absorbent for organic liquids. Journal of Materials Chemistry A, 2014. 2(9): p. 2934-2941.
48. Kim, N.H., T. Kuila, and J.H. Lee, Simultaneous reduction, functionalization and stitching of graphene oxide with ethylenediamine for composites application. Journal of Materials Chemistry A, 2013. 1(4): p. 1349-1358.
49. Xu, Z., et al., Strong, conductive, lightweight, neat graphene aerogel fibers with aligned pores. ACS nano, 2012. 6(8): p. 7103-7113.
50. Li, N., et al., Three-dimensional graphene foam as a biocompatible and conductive scaffold for neural stem cells. Scientific reports, 2013. 3(1): p. 1604.
51. Zhang, X., et al., Mechanically strong and highly conductive graphene aerogel and its use as electrodes for electrochemical power sources. Journal of Materials Chemistry, 2011. 21(18): p. 6494-6497.
52. Marcano, D., et al., Improved synthesis of graphene oxide. ACS Nano 4:4806-4814. ACS nano, 2010. 4: p. 4806-14.
53. Kang, M.S., et al., Graphene oxide-functionalized nanofibre composite matrices to enhance differentiation of hippocampal neuronal cells. Materials Advances, 2020. 1(9): p. 3496-3506.
54. Qian, Y. and C. Fan. Multilayer integration manufacture of graphene oxide based nerve scaffold. in IOP Conference Series: Materials Science and Engineering. 2019. IOP Publishing.